

Article

# Influence of Ammonium Sulfate Seed Particle on Optics and Compositions of Toluene Derived Organic Aerosol in Photochemistry

Tingting Lu <sup>1</sup>, Mingqiang Huang <sup>1,\*</sup> , Weixiong Zhao <sup>2</sup>, Changjin Hu <sup>2</sup>, Xuejun Gu <sup>2</sup> and Weijun Zhang <sup>2,\*</sup>

<sup>1</sup> Fujian Province Key Laboratory of Modern Analytical Science and Separation Technology, College of Chemistry & Chemical Engineering and Environment, Minnan Normal University, Zhangzhou 363000, China; lutingt215@163.com

<sup>2</sup> Laboratory of Atmospheric Physico-Chemistry, Anhui Institute of Optics and Fine Mechanics, Chinese Academy of Sciences, Hefei 230031, China; wxzhaoaiofm@gmail.com (W.Z.); hucjiaiofm@gmail.com (C.H.); xjguaiofm@gmail.com (X.G.)

\* Correspondence: huangmingqiang@mnnu.edu.cn (M.H.); wjzhangaiofm@gmail.com (W.Z.); Tel.: +86-596-2591-445 (M.H.); Fax: +86-596-2026-037 (M.H.)

Received: 15 July 2020; Accepted: 8 August 2020; Published: 10 September 2020



**Abstract:** Aromatic secondary organic aerosol (SOA) particles are known to contribute to radiative forcing and light absorption of atmosphere. However, the complex refractive index (CRI), single-scattering albedo (SSA) and other optical parameters of aromatic SOA are not well understood. SOA generated from photooxidation of toluene with a variety concentration of ammonium sulfate ((NH<sub>4</sub>)<sub>2</sub>SO<sub>4</sub>) seed particles in a smog chamber were investigated in the current study. The real part CRI of toluene SOA without seeds derived and based on aerosol albedometer measurements is  $1.486 \pm 0.002$  at  $\lambda = 470$  nm, showing a good agreement with available experimental data, and its SSA was measured to be  $0.92 \pm 0.02$  at  $\lambda = 470$  nm, indicating that the SOA particles without seeds have strong scattering ability. The SSA of SOA formed in the presence of  $300 \mu\text{g}/\text{m}^3$  (NH<sub>4</sub>)<sub>2</sub>SO<sub>4</sub> seed was  $0.81 \pm 0.02$  at  $\lambda = 470$  nm, less than the SSA of SOA without seed. SSA of SOA decreased, while the imaginary part of CRI (k) of SOA increased with increasing concentration of (NH<sub>4</sub>)<sub>2</sub>SO<sub>4</sub> seed, demonstrating that the adsorption capacity of SOA formed in the presence of (NH<sub>4</sub>)<sub>2</sub>SO<sub>4</sub> seed is enhanced. Different from the carboxyl compounds measured in the SOA without seed, imidazoles with strong chromophores of C=N that are responsible for the light absorption were detected as the principal constituents of SOA formed in the presence of (NH<sub>4</sub>)<sub>2</sub>SO<sub>4</sub> seed. These would provide valuable information for discussing the optics and components of aromatic SOA in the urban atmosphere containing a high concentration of (NH<sub>4</sub>)<sub>2</sub>SO<sub>4</sub> fine particles.

**Keywords:** secondary organic aerosol; complex refractive index; single-scattering albedo; brown carbon; imidazoles

## 1. Introduction

The photooxidation of toluene and other monocyclic aromatic compounds from anthropogenic emission sources leads to the formation of semi- and non-volatile oxygenated compounds, which result in secondary organic aerosol (SOA) particles [1,2]. Interest in SOA has been renewed because of its contribution to radiative balance and visibility degradation [3–5]. Generally, the complex refractive index (CRI) and single-scattering albedo (SSA) are used to characterize the fundamental optical parameters of aerosol particles. CRI is expressed as  $m = n + i k$ ,  $n$  and  $k$  is the real and imaginary part, corresponding to the scattering and absorption of aerosol particles, respectively. SSA is the ratio

of aerosol scattering ( $\alpha_{scat}$ ) to extinction ( $\alpha_{ext}$ , the sum of scattering and absorption) coefficient [6]. However, the CRI and SSA of aromatic SOA are still poorly characterized, due to the inherent complexity in aerosol composition and difficulty in accurate measurement of particulate intrinsic optics.

Cavity ring down spectroscopy (CRDS) has been employed in several chamber studies for the investigation of the CRI of aromatic SOA particles generated in the presence of NO<sub>x</sub>. For toluene SOA particles, Nakayama et al. [7,8] determined the *n* value of SOA particles to be 1.483 at 532 nm, while the imaginary part of CRI, *k*-value was observed to increase with increasing NO<sub>x</sub> concentration. Li et al. [9,10] measured that the real part of CRI of aromatic SOA particles at 532 nm fall in 1.38–1.59, and attributed the decrease of real CRI to the gas-phase partitioning. The real CRI of *m*-xylene SOA formed without seed and in presence of (NH<sub>4</sub>)<sub>2</sub>SO<sub>4</sub> seed decreased as time gone on, when CRI was nearly stable, the real part value of CRI for *m*-xylene SOA was found to decrease by 0.09 and 0.15 compared to the earliest formed SOA, respectively [10]. However, CRDS applied in the work by Nakayama et al. [7,8] and Li et al. [9,10] operated at 532 nm, and the gaseous absorption may bias the extinction result [11]. Additionally, aerosol SSA is not measured in these experiments. Fortunately, the aerosol albedometer can measure the real-time particle optical parameters, such as direct SSA and retrieved CRI [6]. The albedometer generally includes an integrating sphere and incoherent broadband cavity-enhanced absorption spectroscopy (IBBCEAS) for detecting  $\alpha_{scat}$  and  $\alpha_{ext}$ ; CRI and SSA can be acquired simultaneously. IBBCEAS can quantitatively measure gaseous absorption and aerosol extinction; gaseous absorption was subtracted for accurate measurement of  $\alpha_{ext}$  coefficient [12,13]. Recently, our group has developed an albedometer based on IBBCEAS combined with integrating sphere, and measured the SSA of polystyrene latex, ammonium sulfate particles, the optical properties of fine particles and columnar aerosol in Beijing successfully [14–16].

The ubiquitous inorganic fine particles contribute substantially to SOA transformation by providing condensation surface in gas-particle partitioning, modifying reaction environment, involving reactions, or promoting their deposition [17,18]. Atmospheric fine particle pollution is serious in the urban areas of China. The average mass concentrations of particles are in the range of 100–300  $\mu\text{g m}^{-3}$  during haze days in mega-cities of China [19,20]. Ammonium sulfate ((NH<sub>4</sub>)<sub>2</sub>SO<sub>4</sub>) is the major constituent of fine particles during haze days [21]. (NH<sub>4</sub>)<sub>2</sub>SO<sub>4</sub> fine particles can act as efficient seeds to promote SOA formation, mainly due to their large specific surface area. Moreover, the presence of seed particles shall change the optical and chemical results of SOA. Although the real part of CRI of aromatic SOA have been measured [7–10], and the real CRI of *m*-xylene SOA formed in presence of (NH<sub>4</sub>)<sub>2</sub>SO<sub>4</sub> seed was observed to decrease with reaction time [10], no investigations on the influences of (NH<sub>4</sub>)<sub>2</sub>SO<sub>4</sub> seed on the SSA of SOA are performed. Thus, experiments were carried out to measure the SSA of toluene SOA formed without, and in the presence of, (NH<sub>4</sub>)<sub>2</sub>SO<sub>4</sub> seed in the current study. Moreover,  $\alpha_{scat}$  and  $\alpha_{ext}$  coefficients were detected by the aerosol albedometer in real-time, and SSA ( $=\alpha_{scat}/\alpha_{ext}$ ) of the toluene SOA particles were obtained immediately. Additionally, the optical and chemical properties of SOA were further characterized by ultraviolet-visible (UV-Vis) spectrometer and mass spectrometer. The effects of (NH<sub>4</sub>)<sub>2</sub>SO<sub>4</sub> seed on the optical parameters and the compositions of SOA are discussed in detail.

## 2. Experiments

### 2.1. Material

Toluene (>99%) and H<sub>2</sub>O<sub>2</sub> (30%) were supplied by Sigma-Aldrich Chemistry Corporation, Germany. Ammonium sulfate (99.9%) and methanol (>99%) were obtained from The Third Reagent Factory of Tianjin.

Seed particles were generated by aspirating the 4 g/L (NH<sub>4</sub>)<sub>2</sub>SO<sub>4</sub> solution via the atomizer (TSI Inc, Shoreview, MN, USA, Model 3076), passed through the dryer (TSI Inc, Shoreview, MN, USA, Model 3062) and a neutralizer (TSI Inc, Shoreview, MN, USA, Model 3054) successively, then introduced

into the chamber [22,23]. The mean diameter of the  $(\text{NH}_4)_2\text{SO}_4$  seed was  $\sim 100$  nm, and seed was established at a certain concentration by controlling the filling time of the seed particles into the chamber.

## 2.2. Toluene SOA Particles Formation without and in Presence of $(\text{NH}_4)_2\text{SO}_4$ Seed

Formation of toluene SOA particles without and in the presence of different concentration of  $(\text{NH}_4)_2\text{SO}_4$  seed was performed in a 850 L chamber [22,23]. After flushing the chamber, toluene,  $\text{H}_2\text{O}_2$  and  $(\text{NH}_4)_2\text{SO}_4$  seed were delivered into the chamber, which was then filled with zero air to full volume. The concentration of toluene and  $\text{H}_2\text{O}_2$  in the chamber was fixed at 600 and 3000 ppb, respectively. Eight experiments were performed without and in presence of  $(\text{NH}_4)_2\text{SO}_4$  seed in the concentration of 25, 50, 100, 150, 200, 250 and 300  $\mu\text{g}/\text{m}^3$ , respectively. The temperature in the chamber was kept at about  $300 \pm 2$  K, while relative humidity (RH) was  $25 \pm 2\%$  for all the experiments. Two small fans were installed inside the flange of the chamber to mix the gases, which ensures the uniform mixing of chemical compounds in the chamber. Four UV lamps were turned on to irradiate  $\text{H}_2\text{O}_2$  to generate OH radicals [24], which initiated the photooxidation of toluene to form SOA. As illustrated in Figure 1, the concentrations of  $\text{NO}_x$ , toluene, the mass concentration and optics of SOA particles in the chamber was detected using NO- $\text{NO}_2$ - $\text{NO}_x$  analyzer (Thermo Fisher Scientific Inc, Walsham, MA, USA, Model 42i), GC-FID (Agilent Technologies Inc, Palo Alto, CA, USA, Model 7820A), scanning mobility particle sizer (SMPS, TSI Inc, Shoreview, MN, USA, Model 3080L Differential Mobility Analyzer (DMA), Model 3775 Condensation Particle Counter (CPC)) and aerosol albedometer, respectively. Each experiment was conducted for three times, and the average of the results was used as the final data. It is worth noting that no  $\text{NO}_x$  was added for better investigating the effect of  $(\text{NH}_4)_2\text{SO}_4$  seed aerosol on the optical parameters of toluene SOA. The  $\text{NO}_x$  concentration measured by NO- $\text{NO}_2$ - $\text{NO}_x$  analyzer is less than 1 ppb in the whole reaction process. Thus, the  $\text{NO}_x$  concentration in the chamber is not analyzed in this study.

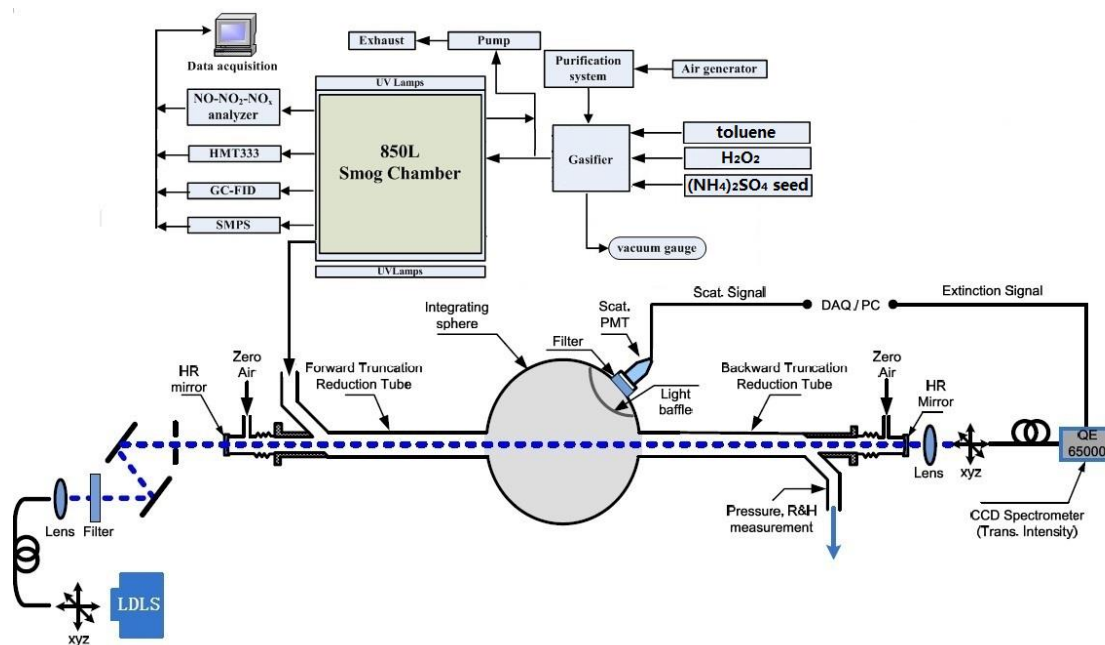


Figure 1. Schematic diagram of the aerosol albedometer and chamber.

## 2.3. Aerosol Albedometer

As displayed in Figure 1, light (190–2100 nm) emitted from a laser-driven light source (LDLS) was coupled into the optical fibers, and passed through the collimators and a 450 nm-centered bandpass filter (Thorlabs FB 450-40, full-width at half-maximum (FWHM) of 40 nm). Thus, light of 410–490 nm was entered into the optical cavity. The cavity includes integrating sphere, truncation reduction tubes

and highly reflective (HR) mirrors. The sphere manufactured with aluminum was separated into two hemispheres, and each hemisphere has a hole for the probe light beam. Moreover, a hole in the side wall is used to measure the scattered signal. SOA particles were introduced into the optical cavity via the forward truncation reduction tube, and then by encountering and interacting with the light in integrating sphere, the generated scattering signal was detected with a photomultiplier tube (PMT). A light baffle was utilized to eliminate the stray light, and a 470 nm-centered (FWHM of 9 nm) bandpass filter was used to prevent the scattered light from directly reaching the PMT. The PMT signal was acquired with a data acquisition card, which provided an integrated scattering signal over 465–474 nm. Meanwhile, the exited light was coupled into the fiber and sent to the CCD spectrometer to measure the extinction signal. The scattering and extinction coefficient at 470 nm was deduced as an averaged scattering and extinction value in the range of 465–474 nm, and utilized for data analysis [14].

#### 2.4. Characterization Compositions of Toluene SOA

After 4 h photooxidation, the toluene SOA particles were collected onto the polytetra fluoroethylene membrane filter and extracted into 5 mL 2% methanol water solution with 30 min sonication [25]. A secondary extraction was performed to confirm that the primary extraction was complete when the absorption spectrum of its extraction is approximately a straight line. The extraction was filtrated with syringe organic filter (33 mm × 0.22 µm, Millipore Corp, Billerica, MA, USA) before the UV-Vis and liquid chromatography-mass spectrometer (LC-MS) measurements. The double beam UV-6100S spectrophotometer (Mapada Instruments, Shanghai, China) was utilized to determine the ultraviolet-visible spectrum of extract solution, with 2% methanol water solution as the reference solution. Moreover, extract solutions were measured by LC-MS with electrospray ionization (ESI) (Agilent Technologies Inc, Palo Alto, CA, USA, Model 1200 and 6320). The autosampler injected the extract sample (20 µL) into the LC system, which introduced the sample into the ESI source region. The extract sample was detected without LC column. The mobile phase was ultra-pure water and methanol (1:1 *v/v*), with the rate of 0.20 mL/min. The extract solutions were analyzed in 50–1000 amu of the negative mode with a fragmentor voltage of 40 V and a capillary voltage of 3000 V. N<sub>2</sub> was the drying gas (350 °C, 24 psig, 10 L/min). The mass spectra were recorded on Agilent software (Chemstation Rev.b.01.03) and exported to Excel for statistical analysis and interpretation [25].

It should be noted that we have not phased out the effect of salt in UV-Vis and subsequent MS measurements of the toluene-SOA extraction. According to the experimental results of Bone et al. [26], imidazoles formed via the aqueous reaction with limonene SOA and NH<sub>4</sub><sup>+</sup> ion over days. Toluene SOA particles were extracted and detected by UV-Vis and LC-MS immediately, so the effect of (NH<sub>4</sub>)<sub>2</sub>SO<sub>4</sub> on the aqueous reaction was negligible. In addition, the *m/z* of sulfate was 48, and the toluene-SOA extraction was detected in 50–1000 amu of the negative mode, thus, (NH<sub>4</sub>)<sub>2</sub>SO<sub>4</sub> in the solution would not affect the measurement of chemical components of SOA.

### 3. Results

#### 3.1. Validation of the Retrieved CRI from the Albedometer

The accuracy and precision of the retrieved CRI, scattering and extinction coefficient from the cavity-enhanced albedometer were tested and evaluated using laboratory-generated mono-disperse polystyrene latex (PSL) particles and polydisperse ambient particles in our previous published papers [13–15]. PSL particles were generated with the atomizer (TSI Inc, Shoreview, MN, USA, Model 3076), and 200, 240, 300 and 400 nm particles were selected by the classifier (TSI Inc, Shoreview, MN, USA, Model 3080L) and supplied to the albedometer to measure the scattering ( $I_{scat}$ ) and extinction ( $I_{trans}$ ) signal, respectively. It should be noted that a small number of multiplied charged particles emerged from the differential mobility analyzer (DMA) selector. These particles were characterized by the tandem DMA method suggested by Bueno et al. [27], and the error of aerosol extinction cross section caused by multiply charged particles was estimated to be 5–20% for the particle diameters smaller

than 300 nm, and less than 5% for the particle diameters larger than 400 nm [13]. As suggested by Washenfelder et al. [28] and Thompson et al. [29], the extinction ( $\alpha_{ext}$ ) and scattering ( $\alpha_{scat}$ ) coefficient can be calculated from the measured  $I_{scat}$  and  $I_{trans}$ . The CRI can be retrieved from the simultaneous measurement of  $\alpha_{ext}$  and  $\alpha_{scat}$  coefficients, subsequently, and the detailed retrieval algorithm was presented in our previous works [13,14]. The retrieved CRI of PSL particles was  $m = 1.676 + i 0.015$  via the scattering signal and  $m = 1.674 + i 0$  via the extinction signal at  $\lambda = 470$  nm, which agreed with the reported result of  $1.633 + i 0.005$  at  $\lambda = 420$  nm from Washenfelder et al. [28], and  $1.627 + i 0.005$  at  $\lambda = 560$  nm provided by Miles et al. [30] However, the imaginary part value of PSL particles retrieved from the scattering channel was larger than these reported values, which may be due to the large internal volume, the longer residual time and the greater agglomeration effect on small particles. The potential uncertainty for the retrieved CRI value was about 5% and 3% via the scattering and extinction signal, respectively [14].

Polydisperse ambient particles measurements were performed outside the laboratory for 24 h. The scattering, extinction coefficients and SSA of the ambient air were measured with the aerosol albedometer, and the scattering coefficients are compared with the measurements from the TSI 3563 integrating nephelometer. A good agreement between the albedometer and the TSI nephelometer is observed [14], demonstrating that albedometer can measure  $\alpha_{ext}$ ,  $\alpha_{scat}$  and SSA of polydisperse aerosol particles simultaneously. Simultaneous measurement of  $\alpha_{ext}$  and  $\alpha_{scat}$  coefficients provides an approach for retrieval of CRI. The detailed retrieval algorithm has been presented in our previous paper [15]. The total uncertainty for the retrieved real CRI value of polydisperse aerosol particles was estimated to be less than 3% and 2% via the scattering and extinction signal, respectively. Additionally, the relative uncertainty for the imaginary part of CRI was estimated to be between 15% and 20% for the k-value less than 0.010, and less than 7% for the k-value greater than 0.010 from the scattering channel, while the uncertainty of the associated imaginary CRI value was better than 10 % for the k-value less than 0.010, and less than 5% for the k-value greater than 0.010 through the extinction channel. The total uncertainty in the measurement of SSA was estimated to be less than 5% [13–15].

### 3.2. Optics of SOA without and in Presence of $(NH_4)_2SO_4$ Seed

The mass concentration and optics of SOA without  $(NH_4)_2SO_4$  seed were measured firstly. Unless mentioned otherwise, the optical properties of SOA were derived at 470 nm. Similar to our previous work, the density of  $1.23 \text{ g/cm}^3$  was used to estimate the mass concentration of particle measured by SMPS [31]. Wall loss was described as a first order process dependent on the loss coefficient,  $k_{dep}(d_p)$ :

$$k_{dep}(d_p) = ad_p^b + c/d_p^d \quad (1)$$

where  $a$ ,  $b$ ,  $c$ , and  $d$  were optimized to be  $4.17 \times 10^{-13}$ , 4.66, 10.18, and 0.75, respectively [22,31]. The mass concentration of SOA was corrected for wall loss by fitting the particle number concentration decay at the end of the experiment. For the mixed gases of 600 ppb toluene and 3000 ppb  $H_2O_2$ , the corrected mass concentration, particle number concentration, mean diameter, SSA and other optical parameters of toluene SOA with different reaction time measured by SMPS and albedometer are shown in Figures 2 and 3. In the first 5 min of the photooxidation time, only few particles with a corrected mass concentration of  $1.5 \mu\text{g/m}^3$  was observed. OH radicals generated from the photolysis of  $H_2O_2$  undergo hydrogen extraction and addition reactions with toluene to form semi- and non-volatile products. According to the theory of gas/particle partitioning [32], these gaseous products nucleate homogeneously only after exceeding their saturation concentration. So, nearly no SOA particles would be formed until sufficient toluene had reacted to generate gaseous concentrations that exceed saturation concentration. Meanwhile, afterward, the fine particles less than 100 nm increased sharply. Within 5–35 min, the particle number concentration of toluene SOA increased from  $\sim 200 \text{ pt/cm}^3$  to  $\sim 150,000 \text{ pt/cm}^3$ , the corrected mass concentration of SOA increased from  $1.5 \mu\text{g/m}^3$  to  $74 \mu\text{g/m}^3$ , and the scattering and extinction coefficient measured by the albedometer increased to about 450 and  $480 \text{ Mm}^{-1}$ ,

respectively. In the following 35–65 min, the particle number concentration of SOA decreases and the particle size increases gradually, due to more gaseous products condensed on the pre-existing particles and collision between fine particles. At about 65 min, the particle number concentration of toluene SOA decreases to  $\sim 100,000$   $\text{pt}/\text{cm}^3$ , the mean diameter increases to 240 nm, the corrected mass concentration of SOA increases to  $145 \mu\text{g}/\text{m}^3$ , and  $\alpha_{\text{scat}}$  and  $\alpha_{\text{ext}}$  reach the maximum value of 680 and  $740 \text{ M m}^{-1}$ , respectively. Thereafter, no toluene react to form new particles; the size distribution of SOA remained basically unchanged. However, due to turbulence and gravity deposition, toluene SOA particles deposited on the chamber wall [22,23], resulting in a gradual decrease in the number concentration, scattering coefficient and absorption coefficient of toluene SOA particles, as illustrated in Figure 3. As the wall loss is the main factor in reducing the mass concentration of SOA, the corrected mass concentration of SOA was almost constant after 65 min, as shown in Figure 2.

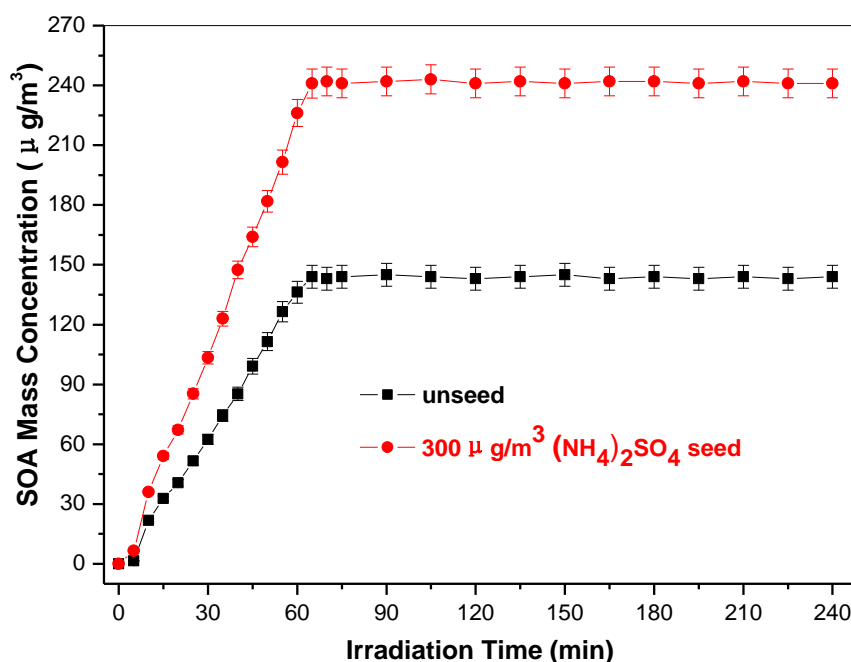


**Figure 2.** The corrected mass concentration of toluene secondary organic aerosol (SOA) formed in absence of seed and in presence of  $300 \mu\text{g}/\text{m}^3$   $(\text{NH}_4)_2\text{SO}_4$  seed as a function of reaction time.

It can be seen from Figure 3 that  $\alpha_{\text{ext}}$ ,  $\alpha_{\text{scat}}$  and SSA of SOA increase with the increasing of particle size. According to the measurement results of GC, toluene in the chamber has been almost completely consumed after 65 min of illumination, after that the mean diameter and size distribution of SOA were maintained almost constantly. Although the wall effect causes the particle number concentration, extinction and scattering coefficient of toluene SOA to decrease gradually, SSA remains substantially unchanged. SSA characterizes the relative strength of the scattering and absorption. Its value ranges from 1 for purely scattering to 0 for completely absorbing particle [6]. The SSA of SOA was measured to be  $0.92 \pm 0.02$ , indicating that toluene SOA particles without  $(\text{NH}_4)_2\text{SO}_4$  seed have strong scattering ability. This was further confirmed by the retrieved CRI from the scattering and extinction channel. The retrieved real and imaginary part of the CRI of the toluene SOA is  $1.486 \pm 0.002$  and  $0.006 \pm 0.001$  via the scattering signal, and  $1.479 \pm 0.002$  and  $0.004 \pm 0.001$  via the extinction signal, respectively, when the size distribution of SOA is kept nearly unchanged. The real CRIs of toluene SOA retrieved from scattering and extinction channels fall well within the range of 1.431–1.498 at  $\lambda = 532 \text{ nm}$  reported by Nakayama et al. [8] and 1.450–1.518 at  $\lambda = 532 \text{ nm}$  measured by Li et al. [9]. It is worth noting that the CRI retrieved by the scattering channel is slightly larger than that obtained by the extinction channel. Since the real CRI of toluene obtained by the scattering channel is closer to the corresponding value (1.518) of toluene SOA with low- $\text{NO}_x$  and  $\text{H}_2\text{O}_2$  was utilized as an OH precursor

performed by Li et al. [9], the CRI retrieved by the scattering channel was shown in Figure 3 and used to investigate the effect of  $(\text{NH}_4)_2\text{SO}_4$  seed on the optical properties of toluene SOA. The imaginary part  $k$  is the characterization of the ability of absorbing light radiation. The larger the  $k$  value, the stronger the light absorption of aerosol particles. The measured  $k$ -value of toluene SOA particles shown in Figure 3 is only  $0.006 \pm 0.001$ , indicating that toluene SOA without  $(\text{NH}_4)_2\text{SO}_4$  seed has weak absorbability and contributes mainly to a cooling effect.

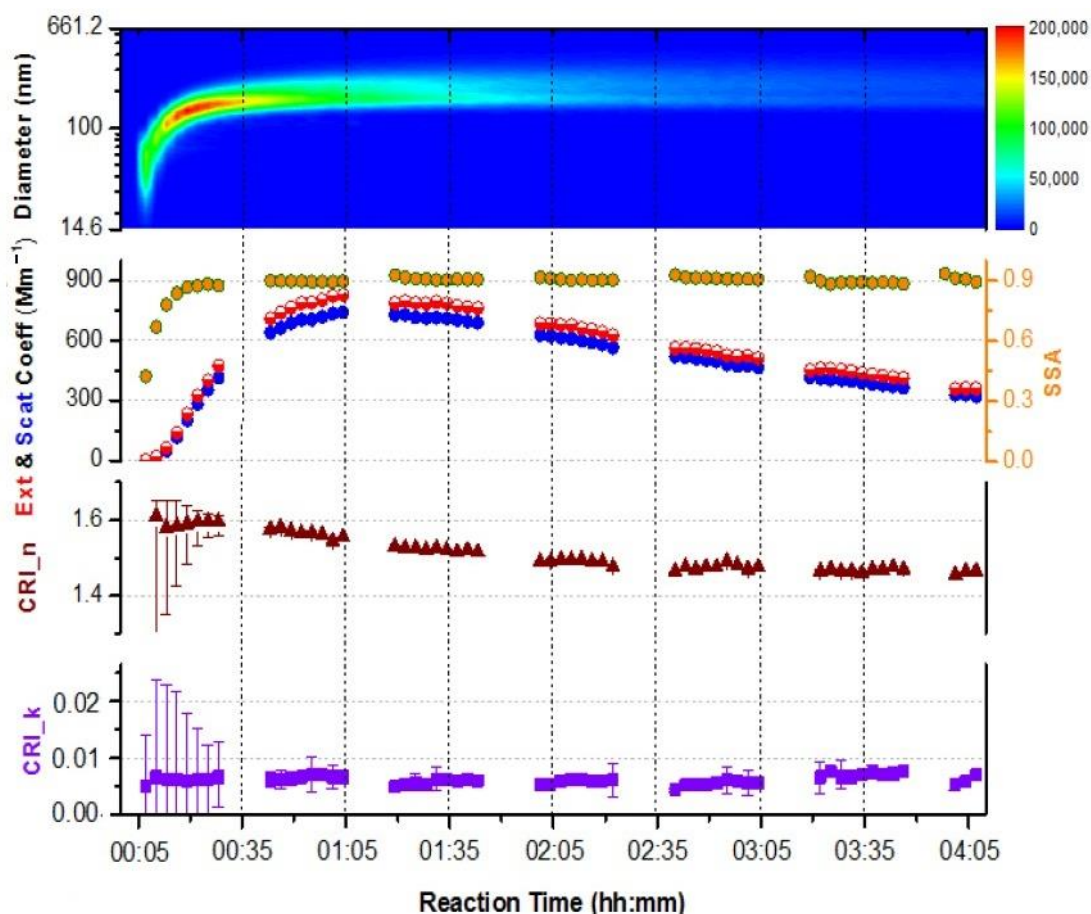


**Figure 3.** The particle number concentration, mean diameter, extinction and scattering coefficients, SSA and complex refractive index (CRI) of SOA without  $(\text{NH}_4)_2\text{SO}_4$  seed as a function of reaction time.

The SSA and CRI of SOA particles formed in the presence of different concentration of  $(\text{NH}_4)_2\text{SO}_4$  seed were measured to explore the influences of  $(\text{NH}_4)_2\text{SO}_4$  seed on the optics of toluene SOA. For the  $(\text{NH}_4)_2\text{SO}_4$  seeded experiments, the corrected mass concentration of SOA was calculated by subtracting the initial seed mass concentration from the wall loss corrected aerosol mass concentration. The obtained curves of the corrected mass concentration, particle number concentration, mean diameter, extinction and scattering coefficients, SSA and CRI of toluene SOA particles formed in the presence of  $300 \mu\text{g}/\text{m}^3$   $(\text{NH}_4)_2\text{SO}_4$  seed with different reaction time displayed in Figures 2 and 4 are similar to the situation without  $(\text{NH}_4)_2\text{SO}_4$  seed. However, the corrected maximum concentration of toluene SOA reached  $242 \mu\text{g}/\text{m}^3$  at 65 min, which was 67% higher than that without seed aerosol, indicating that  $(\text{NH}_4)_2\text{SO}_4$  seed aerosol can promote the formation of toluene SOA. Different from the case without  $(\text{NH}_4)_2\text{SO}_4$  seed where the extinction coefficient is approximately equal to the scattering coefficient, the measured extinction coefficient of toluene SOA formed in the presence of  $300 \mu\text{g}/\text{m}^3$   $(\text{NH}_4)_2\text{SO}_4$  seed is larger than that of scattering coefficient after 65 min of illumination. The measured SSA illustrated in Figure 4 was  $0.81 \pm 0.02$ , less than the SSA of toluene SOA particles without  $(\text{NH}_4)_2\text{SO}_4$  seed of 0.92,

and slightly lower than SSA of biomass burning organic aerosols range in 0.84–0.93 [33], indicating that the toluene SOA formed in the presence of  $(\text{NH}_4)_2\text{SO}_4$  seed had a certain light-absorption capacity.

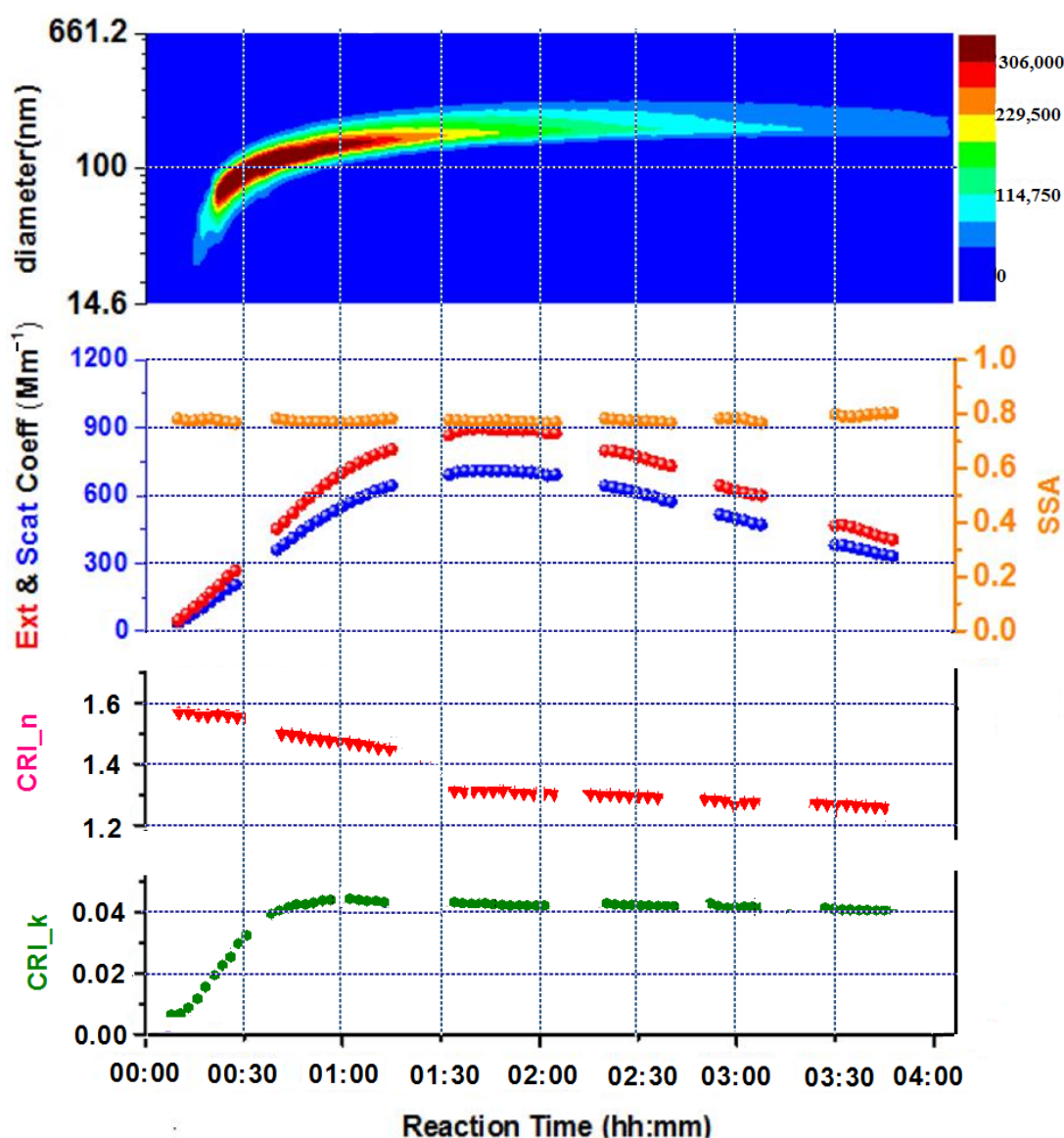


**Figure 4.** The particle number concentration, mean diameter, extinction and scattering coefficients, single-scattering albedo (SSA) and CRI of SOA formed in presence of  $300 \mu\text{g}/\text{m}^3$   $(\text{NH}_4)_2\text{SO}_4$  seed as a function of reaction time.

As shown in Figures 3 and 4, the real CRI of toluene SOA formed in the absence and presence of  $300 \mu\text{g}/\text{m}^3$   $(\text{NH}_4)_2\text{SO}_4$  seed decreased as time went on. The real part value of CRI for toluene SOA without seed was found to decrease from 1.608 to 1.486 when CRI was nearly stable. Furthermore, the real CRI of SOA formed in presence of  $(\text{NH}_4)_2\text{SO}_4$  seed was smaller than that of without seed, and its real CRI decrease from 1.592 to 1.285. Similar to the system of m-xylene SOA performed by Li et al. [10], the relatively low volatile gaseous product of photooxidation of toluene nucleated to generate SOA particles in the absence of seed. As the reaction proceeded, the concentration of organics increased, particles got larger, and volatile products with low CRI would condense on the particles, which led to the real CRI of SOA to decrease with time, as shown in Figure 3. The presence of  $(\text{NH}_4)_2\text{SO}_4$  seed promoted the condensation of volatile organics [10,34], condensation of gaseous products of photooxidation of toluene and further heterogeneous reactions on the surface of seed can

possibly form a core-shell mixing state at RH = 25%. More and more higher volatility products with lower CRI condensed on the particles as time gone on, and the real CRI of SOA formed in presence of  $300 \mu\text{g}/\text{m}^3$   $(\text{NH}_4)_2\text{SO}_4$  seed displayed in Figure 4 decreased significantly when compared to that without seed.

Figure 5 displayed the corrected maximum mass concentration of toluene SOA detected by SMPS, SSA, the real (n) and imaginary (k) part of CRI of SOA measured at different concentrations of  $(\text{NH}_4)_2\text{SO}_4$  seed when the size distribution of SOA particles remains basically unchanged. As shown in Figure 5a, the corrected maximum concentration of toluene SOA at different concentrations of  $(\text{NH}_4)_2\text{SO}_4$  seed is in the range of 166–242  $\mu\text{g}/\text{m}^3$ , which is higher than that without seed (145  $\mu\text{g}/\text{m}^3$ ). It should be noted that, when the concentration of  $(\text{NH}_4)_2\text{SO}_4$  seed aerosol was greater than 200  $\mu\text{g}/\text{m}^3$ , the maximum concentration of toluene SOA did not continue to increase. SSA and real CRI of SOA decrease, while k of SOA increases with the increasing concentration of  $(\text{NH}_4)_2\text{SO}_4$  seed (Figure 5b–d). Similarly, when  $(\text{NH}_4)_2\text{SO}_4$  seed exceeds 200  $\mu\text{g}/\text{m}^3$ , the optical parameters of SOA tend to be stable. The n-value of toluene SOA formed in the presence of  $300 \mu\text{g}/\text{m}^3$   $(\text{NH}_4)_2\text{SO}_4$  seed is 1.285, 14% less than that of without seed (1.486), and the k-value of SOA is 0.042, 6 times larger than SOA generated in absence of  $(\text{NH}_4)_2\text{SO}_4$  seed of 0.006, demonstrating that  $(\text{NH}_4)_2\text{SO}_4$  seed is involved in the photochemical reaction of toluene with OH radicals, resulting in products with light absorbing ability.

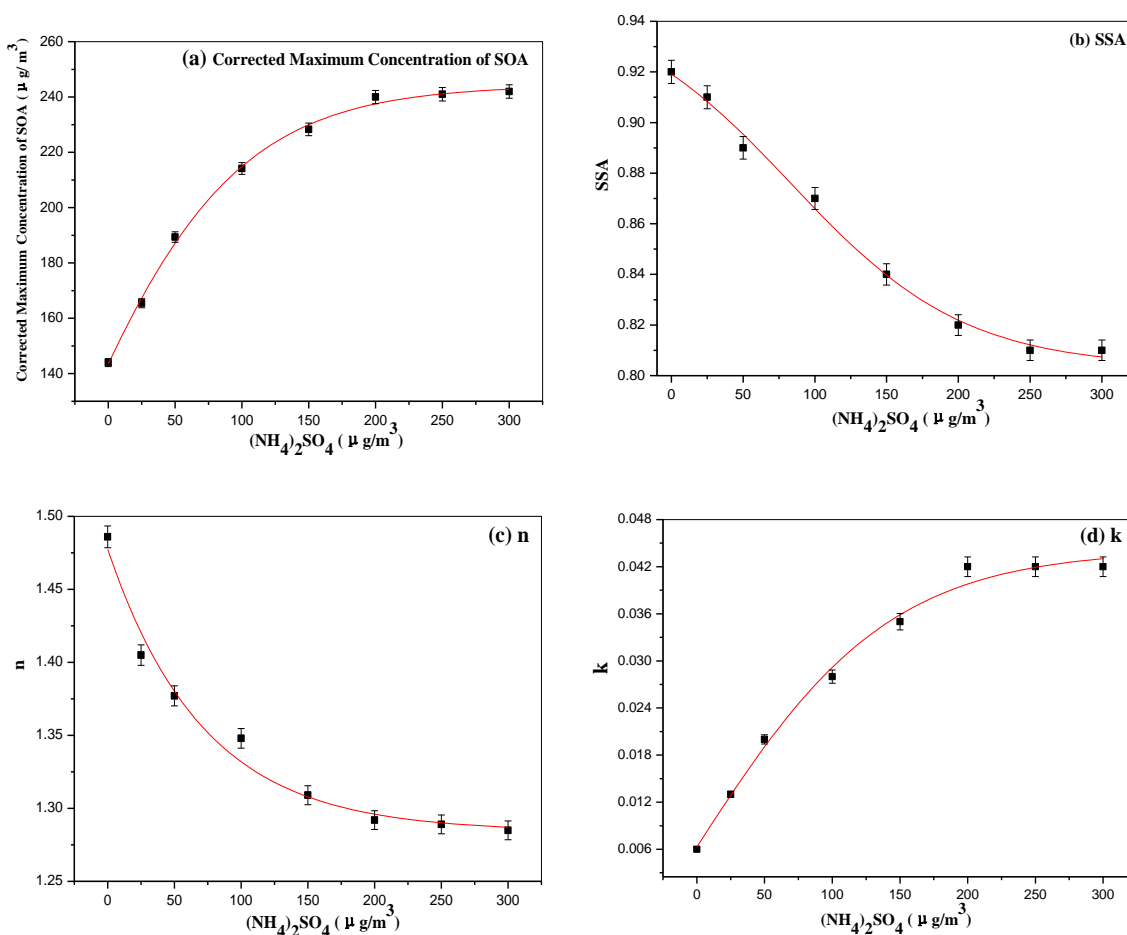


**Figure 5.** The (a) corrected maximum mass concentration (b) SSA (c) n and (d) k of SOA particles measured at different concentrations of  $(\text{NH}_4)_2\text{SO}_4$  seed.

### 3.3. Components of Toluene SOA without and in Presence of $(\text{NH}_4)_2\text{SO}_4$ Seed

The OH-initiated photooxidation of toluene generates methyl-hydroxy-cyclohexadienyl and benzyl radical radical via OH addition and hydrogen abstraction, respectively [35,36]. As shown in

Figure 6, the reactions of the benzyl radical with  $O_2$  led to the generation of benzaldehyde, and the methyl-hydroxy-cyclohexadienyl radical reacts with  $O_2$  by H-abstraction to form cresol and  $O_2$  addition to yield peroxy radical, which undergo a series of reactions to yield 5-methyl-6-oxo-2,4-hexadienal, glyoxal, and other aldehydes. Furthermore, aldehyde products, such as glyoxal, methylglyoxal can further be oxidized to carboxylic acids [37]. As proposed by Suh et al. [38], the reaction channel of methylhydroxycyclohexadienyl radical with  $O_2$  by hydrogen abstraction had been shown to be relatively minor, demonstrating that carboxyl compounds are the principal components of toluene SOA in the absence of  $(NH_4)_2SO_4$  seed. These results are further confirmed by the ESI-MS and UV-Vis spectra of SOA without  $(NH_4)_2SO_4$  seed illustrated in Figures 7 and 8.

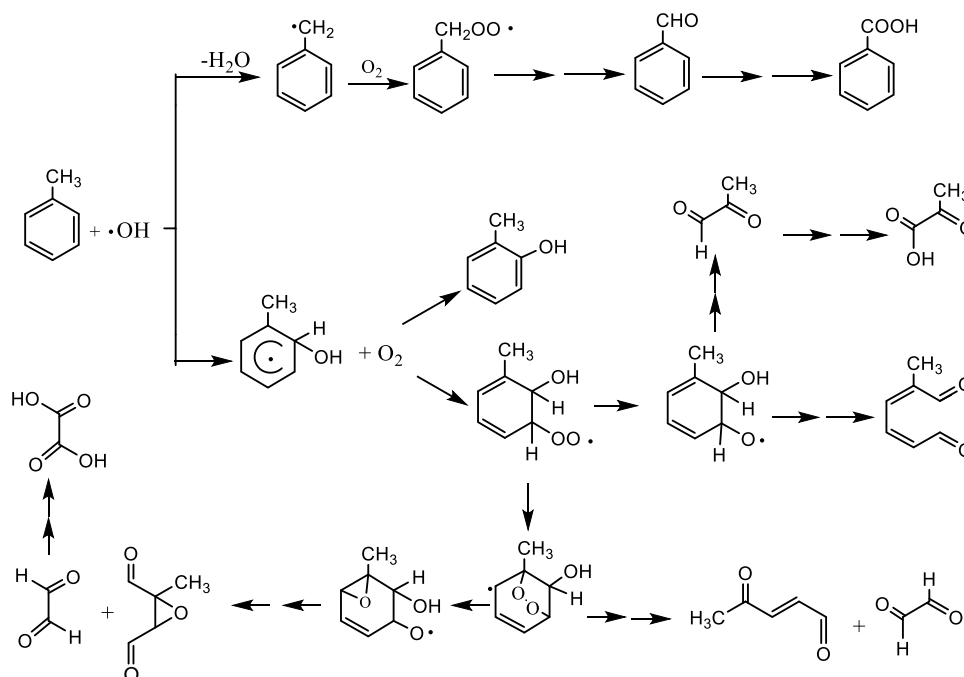


Figure 6. Suggested mechanism for aldehyde and carboxylic productions in photooxidation of toluene.

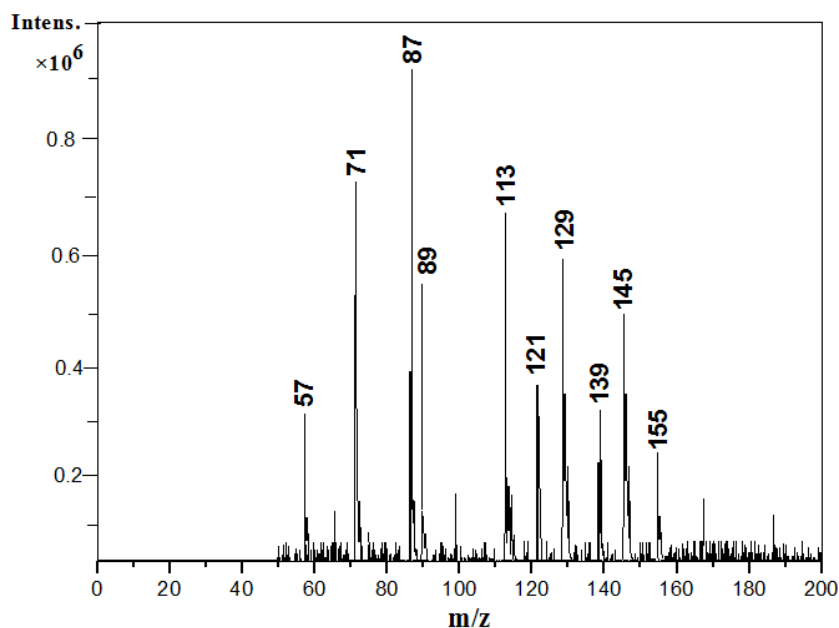
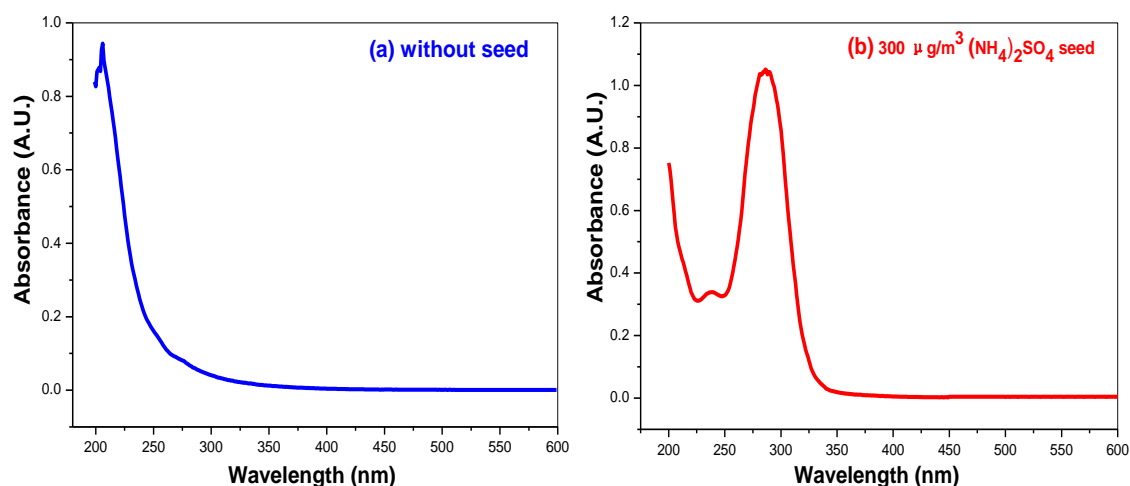


Figure 7. Negative mass spectrum of SOA without  $(NH_4)_2SO_4$  seed.



**Figure 8.** UV-Vis spectra of the SOA (a) without and (b) in presence of  $300 \mu\text{g}/\text{m}^3$   $(\text{NH}_4)_2\text{SO}_4$  seed.

Due to the small volume of our chamber (850 L), coupled with wall effects and other effects, the mass of the collected particulate matter is only tens to hundreds of micrograms, and we cannot accurately measure its mass with the electronic balance (accurate to 0.0001 g). The UV-Vis absorption spectrum was used to qualitatively verify the component of toluene SOA. Therefore, we estimated the mass of the SOA collected on the filter, based on the concentration of the particles measured by SMPS at the end of the reaction. The concentration of toluene SOA without seed at the end of the reaction is about  $60 \mu\text{g}/\text{m}^3$ , the remaining volume in the chamber is about 700 L, and the mass of toluene SOA collected is estimated to be about  $40 \mu\text{g}$ ; the concentration of extract for SOA is about 8 mg/L. As suggested by Carlton et al. [39], ESI deprotonated compounds and the formed negative ions are molecular-related ions  $[\text{M}-\text{H}]^-$ , which provided the information of organic's molecular weight. The  $[\text{M}-\text{H}]^-$  ions of carboxyl compounds, such as glyoxal ( $m/z$  57), methylglyoxal ( $m/z$  71), methylglyoxylic acid ( $m/z$  87), oxalic acid ( $m/z$  89), 4-oxo-2-pentenoic acid ( $m/z$  113) and benzoic acid ( $m/z$  121), 2-methyl-4-oxo-2,3-epoxy-butyric acid ( $m/z$  129), 2-methyl-2,3-epoxy-succinic acid ( $m/z$  139), 5-methyl-6-oxo-2,4-hexadienoic acid ( $m/z$  145) and 5-methyl-2,4-hexadiendioic acid ( $m/z$  155) appear in the ESI-MS shown in Figure 7. In addition, the absorption band at 205 nm of characteristic light absorption of carboxyl compounds [38] emerged in the ultraviolet-visible spectrum of SOA, as displayed in Figure 8a. The formed aldehydes and carboxylic acids contain only C=C and C=O double bonds, and do not contain strong chromophores and auxochromes [40]. Thus, toluene SOA particles without  $(\text{NH}_4)_2\text{SO}_4$  seed have weak light absorption.

Toluene SOA concentration formed in the presence of  $300 \mu\text{g}/\text{m}^3$   $(\text{NH}_4)_2\text{SO}_4$  seed at the end of the reaction is about  $340 \mu\text{g}/\text{m}^3$ , and the mass of collected particles is estimated to be about  $240 \mu\text{g}$ . In order to estimate the mass of the collected toluene SOA formed in the presence of seed,  $300 \mu\text{g}/\text{m}^3$   $(\text{NH}_4)_2\text{SO}_4$  seed was separately prepared for photooxidation reaction. After 4 hours' photooxidation, the particle concentration was about  $250 \mu\text{g}/\text{m}^3$ , and the mass of collected ammonium sulfate was estimated to be about  $175 \mu\text{g}$ . Thus, the mass of collected toluene SOA formed in the presence of  $300 \mu\text{g}/\text{m}^3$   $(\text{NH}_4)_2\text{SO}_4$  seed was about  $65 \mu\text{g}$ , and the concentration of extract for SOA formed in the presence of  $300 \mu\text{g}/\text{m}^3$   $(\text{NH}_4)_2\text{SO}_4$  seed was about 13 mg/L. As suggested by Updyke et al. [41], the mass absorption coefficient (MAC,  $\text{m}^2/\text{g}$ ) can be calculated from the absorbance  $A(\lambda)$  of the SOA extract, with solution mass concentration  $C_{\text{mass}}$  ( $\text{g}/\text{m}^3$ ) measured over pathlength  $b$  (m):

$$\text{MAC}(\lambda) = \frac{A(\lambda) \times \ln 10}{b \times C_{\text{mass}}} \quad (2)$$

Figure 8b gave absorbance of 0.0045 at 470 nm, and the corresponding MAC was estimated to be  $0.080 \text{ m}^2/\text{g}$ , which was comparable to MAC values of brown carbon produced by aging SOA with

NH<sub>3</sub> performed by Updyke et al. [41] This indicated that the measured UV-Vis spectrum can reflect the optical characteristics of toluene SOA.

The UV-Vis absorption profile of toluene SOA formed in the presence of 300 µg/m<sup>3</sup> (NH<sub>4</sub>)<sub>2</sub>SO<sub>4</sub> seed shown in Figure 8b is different from that of without seed. There is a distinctive band at 280 nm in spectra of toluene SOA formed in presence of (NH<sub>4</sub>)<sub>2</sub>SO<sub>4</sub> seed, indicating the generation of new products. The band of 280 nm was also emerged in the spectra of aqueous reaction products of (NH<sub>4</sub>)<sub>2</sub>SO<sub>4</sub> and glyoxal measured by Kampf et al. [42], Lee et al. [43] and Maxut et al. [44] They considered that the chromophores were probably imidazole products formed from the reactions between NH<sub>4</sub><sup>+</sup> and glyoxal, and the n→π\* transition in the C=N of imidazoles was the main contributor to the 280 nm band. As glyoxal and methylglyoxal are the principal α-dicarbonyl gaseous products formed by photooxidation of toluene [36,45], similar reactions to form imidazole compounds may occur after α-dicarbonyls condensate on the surface of (NH<sub>4</sub>)<sub>2</sub>SO<sub>4</sub> seed. Furthermore, the obtained negative mass spectra of toluene SOA formed in the presence of 300 µg /m<sup>3</sup> (NH<sub>4</sub>)<sub>2</sub>SO<sub>4</sub> seed illustrated in Figure 9 contained [M-H]<sup>-</sup> of C<sub>x</sub>H<sub>y</sub>N<sub>n</sub>O<sub>z</sub> family of imidazole derivative compounds. In addition, [M-H]<sup>-</sup> of 67, 81, 95, 123 could be attributed to C<sub>3</sub>H<sub>3</sub>N<sub>2</sub><sup>-</sup>, C<sub>4</sub>H<sub>5</sub>N<sub>2</sub><sup>-</sup>, C<sub>4</sub>H<sub>3</sub>N<sub>2</sub>O<sup>-</sup> and C<sub>6</sub>H<sub>4</sub>N<sub>2</sub>O<sup>-</sup>, respectively, which were also detected by Liu et al. [46] in the experiment of heterogeneous uptake of NH<sub>3</sub> by m-xylene SOA and the previous study of aged benzene SOA formed in presence of (NH<sub>4</sub>)<sub>2</sub>SO<sub>4</sub> seed [23]. These results indicated that imidazoles are the newly formed particulate products of toluene SOA in the presence of (NH<sub>4</sub>)<sub>2</sub>SO<sub>4</sub> seed.

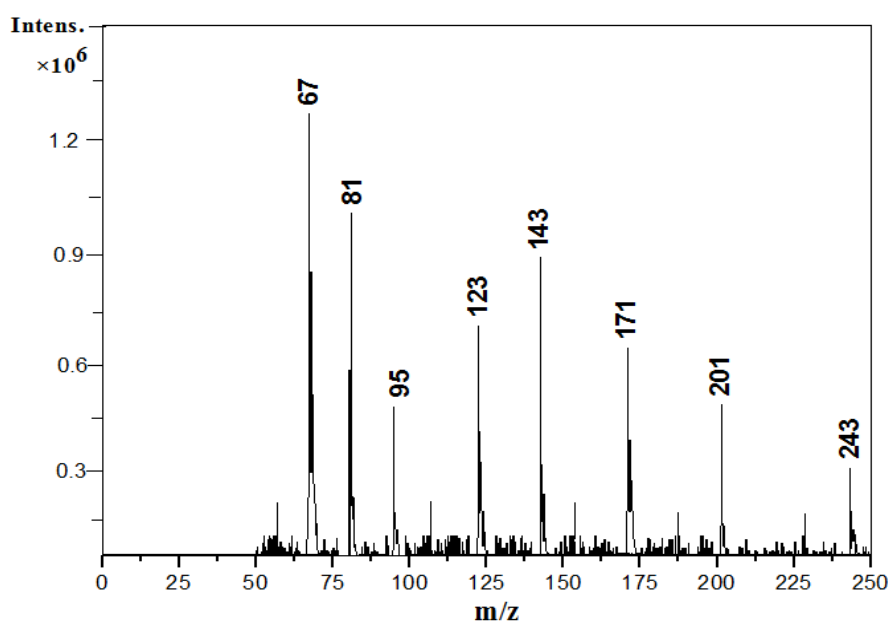
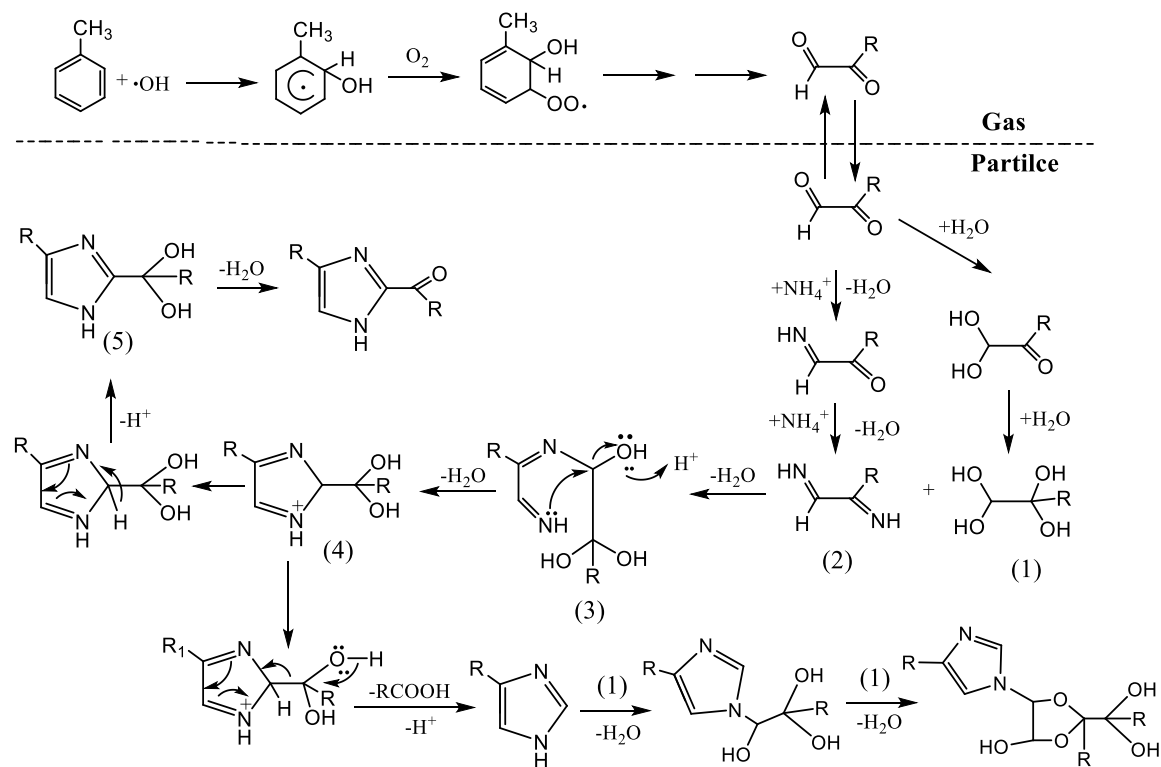


Figure 9. Negative mass spectrum of SOA formed in presence of 300 µg/m<sup>3</sup> (NH<sub>4</sub>)<sub>2</sub>SO<sub>4</sub> seed.

According to the experimental results of Trainic et al. [47], heterogeneous reactions between glyoxal and dehydrated ammonium sulfate cannot occur at RH of 35%. Compared with the reaction system of glyoxal and ammonium sulfate seed performed by Trainic et al. [47], the composition of our reaction system is more complex. In addition to glyoxal, carboxylic acids such as formic acid, acetic acid and glyoxylic acid were also produced from the photooxidation of toluene [36,45]. Some studies have reported that the presence of organics in SOA-coated (NH<sub>4</sub>)<sub>2</sub>SO<sub>4</sub> particles could increase the particles' water uptake compared to that of pure (NH<sub>4</sub>)<sub>2</sub>SO<sub>4</sub> particles, even with RH less than 30% [48–50]. Meyer et al. [50] found that SOA coating enhanced the water uptake of (NH<sub>4</sub>)<sub>2</sub>SO<sub>4</sub> seed, and led to a partially dissolved (NH<sub>4</sub>)<sub>2</sub>SO<sub>4</sub> seed. Thus, (NH<sub>4</sub>)<sub>2</sub>SO<sub>4</sub> seed can partially be hydrated by absorbing water from its covered outer organic layer, with RH of 25% of our reaction system. Additionally, the gaseous carboxylic acid products of toluene condense on the water layer of the

seed to produce acidic aqueous layer for heterogeneous imidazole formation [22]. The gas/particle partitioning of degradation products on seed particle are principal contributions to the formation of toluene SOA formed in presence of  $(\text{NH}_4)_2\text{SO}_4$  seed [46]. When glyoxal, methylglyoxal and other  $\alpha$ -dicarbonyls are partitioned on the  $(\text{NH}_4)_2\text{SO}_4$  seed, heterogeneous acid-catalyzed reactions occur to form imidazole products. Glyoxal and methylglyoxal can be protonated by  $\text{H}^+$  ion and hydrolyzed to tetrol product (1), as displayed in Figure 9. Additionally, the protonated  $\alpha$ -dicarbonyls can react with  $\text{NH}_4^+$  ions to produce diimine product (2). Tetrol product (1) can react with diimine product (2) to form (3) through the dehydration reaction. However, (3) is unstable, N atom attacks C atom, generating (4) after dehydration. Moreover, (4) forms  $\text{HCOOH}$  (or  $\text{CH}_3\text{COOH}$ ) and imidazole ( $m/z$  67) (or 4-methyl-imidazole ( $m/z$  81)) via rearrangement and dehydration reaction. Additionally, (4) occurs rearrangement illustrated in Figure 10 to produce (5), which could be dehydrated to yield imidazole-2-carbaldehyde ( $m/z$  95) (or 4-methyl-imidazole-2-acetaldehyde ( $m/z$  123)). As depicted in Figure 10, the formed imidazole (or 4-methyl-imidazole) can subsequently interact with (1) to produce hydrated N-glyoxal substituted imidazole ( $m/z$  143) (or hydrated N-methylglyoxal substituted 4-methyl-imidazole ( $m/z$  171)), hydrated glyoxal dimer substituted imidazole ( $m/z$  201) (or hydrated methylglyoxal dimer substituted 4-methyl-imidazole ( $m/z$  243)), respectively [42–44].



**Figure 10.** Suggest mechanism for imidazole compounds.

The high concentration of  $(\text{NH}_4)_2\text{SO}_4$  seed provides more surface area for condensation and reaction of gaseous  $\alpha$ -dicarbonyls. Thus, the content of imidazoles in SOA increases with the concentration of seed aerosol, which leads to the increase of absorptivity of SOA with the concentration of seed aerosol, as shown in Figure 5. It is noteworthy that the concentration of toluene,  $\text{H}_2\text{O}_2$  and other conditions are basically unchanged in all experiments, and the amount of the formed  $\alpha$ -dicarbonyls is also nearly constant for each experiment. When  $(\text{NH}_4)_2\text{SO}_4$  seed is increased to a certain concentration ( $200 \mu\text{g}/\text{m}^3$ ), all the  $\alpha$ -dicarbonyls are consumed completely, and the formation of imidazoles would not increase with the increasing concentration of  $(\text{NH}_4)_2\text{SO}_4$  seed. Thus, the optical properties of toluene SOA remain basically unchanged when  $(\text{NH}_4)_2\text{SO}_4$  seed exceeds  $200 \mu\text{g}/\text{m}^3$ , as illustrated in Figure 5.

It should be pointed out that, due to the low sensitivity of UV-Vis spectrophotometer with 1 cm optical length, almost no absorption of toluene SOA is measured at 380 nm, as shown in Figure 8. However, the albedometer with 3.7 km effective optical path can detect the absorption of toluene SOA with 465–474 nm [14]. Compared to the studies of Nakayama et al. [7,8] and Li et al. [9,10], the present study extended  $(\text{NH}_4)_2\text{SO}_4$  seed to  $300 \mu\text{g}/\text{m}^3$ , and the optics of SOA were detected by aerosol single-scattering albedometer in real-time. The measured SSA of toluene SOA formed in the presence of  $300 \mu\text{g}/\text{m}^3$   $(\text{NH}_4)_2\text{SO}_4$  seed was  $0.81 \pm 0.02$ , showing a certain light-absorption capacity [6,40]. Additionally, the SSA of toluene SOA was observed to decrease from 0.91 to 0.81, while the imaginary part of CRI (k) was found to increase from 0.013 to 0.042 with increasing the  $(\text{NH}_4)_2\text{SO}_4$  seed concentration from 25 to  $300 \mu\text{g}/\text{m}^3$ , demonstrating that the adsorption capacity of toluene derived SOA increased with the increasing concentration of  $(\text{NH}_4)_2\text{SO}_4$  seed. From absorption and mass spectrum of SOA, we confirmed that the decrease of SSA and increase of k caused by  $(\text{NH}_4)_2\text{SO}_4$  seed are due to the increase of imidazoles in SOA. The C=N chromophores of imidazoles enhance the absorption capacity of SOA. According to the UV-Vis absorption spectra shown in Figure 8, toluene SOA formed in the presence of  $(\text{NH}_4)_2\text{SO}_4$  seed has strong absorption ability in the UV range. Owing to the rate of global production of anthropogenic SOA is larger than biomass burning organic aerosols [51]; aromatic SOA in the urban atmosphere containing high concentrations of  $(\text{NH}_4)_2\text{SO}_4$  fine particles may contribute remarkably to climate forcing.

#### 4. Conclusions

The aromatic SOA in the urban atmosphere with high concentrations of  $(\text{NH}_4)_2\text{SO}_4$  seed are considered as a potential major component of brown carbon. The toluene SOA particles were formed with different concentrations of  $(\text{NH}_4)_2\text{SO}_4$  seed in the chamber, and measured by the aerosol single-scattering albedometer, spectroscopic and mass spectrometer in the present study. The detected SSA of SOA formed in the presence of  $(\text{NH}_4)_2\text{SO}_4$  seed is less than the SOA without seed, and the imaginary part of CRI (k) was found to increase with increasing the concentration of  $(\text{NH}_4)_2\text{SO}_4$  seed. Compared with the SOA without seed, imidazoles inferred from absorption and mass spectra of SOA formed in the presence of  $(\text{NH}_4)_2\text{SO}_4$  seed were confirmed to be responsible for the decreased SSA and increased k. As the SSA of SOA formed in presence of  $(\text{NH}_4)_2\text{SO}_4$  seed is lower than BBOA detected at  $\lambda = 550 \text{ nm}$ , while absorption capacity in the ultraviolet range is higher and the rate of production of SOA is larger than BBOA, the anthropogenic SOA with high concentration of  $(\text{NH}_4)_2\text{SO}_4$  fine particles may contribute to the radiative balance in urban atmosphere. Although the concentration of  $(\text{NH}_4)_2\text{SO}_4$  seed in the chamber is higher than actual atmosphere, the influence of high mass concentration of  $(\text{NH}_4)_2\text{SO}_4$  seed is still expected to be prevalent in Chinese Urban atmosphere as organic aerosol mass loading is low, under which condition the incidence of mass concentration of  $(\text{NH}_4)_2\text{SO}_4$  effect could be high [52]. These experimental results could be utilized to improve the estimation of radiative forcing of anthropogenic SOA in some regions. Nevertheless, the components of SOA were qualitatively measured by UV-Vis and LC-MS; a suitable chromatographic column should be selected to separate and quantitatively analyze the constituents of toluene SOA. Additionally, SOA were generated in the presence of  $(\text{NH}_4)_2\text{SO}_4$  seed with a relative humidity (RH) of  $25 \pm 2\%$ ; the effects of RH on the optics of aromatic SOA should be carried out in future experiments.

**Author Contributions:** Conceptualization, M.H. and W.Z. (Weijun Zhang); methodology, W.Z. (Weijun Zhang) and W.Z. (Weixiong Zhao); software, X.G.; validation, M.H. and W.Z. (Weijun Zhang); formal analysis, W.Z. (Weixiong Zhao) and C.H.; data curation, T.L.; writing—original draft preparation, T.L.; writing—review and editing, M.H.; project administration, M.H.; funding acquisition, M.H. and C.H. All authors reviewed and commented on the paper. All authors have read and agreed to the published version of the manuscript.

**Funding:** This research was funded by the National Natural Science Foundation of China (No. 41575118, 41575126, 41305109), the Key Project of Foundation of Fujian Province of China (No.2020J06018), the science and technology project of Minnan Normal University (No. 4201-L11805).

**Conflicts of Interest:** The authors declare no conflict of interest.

## References

1. Drozd, G.T.; Zhao, Y.; Saliba, G.; Frodin, B.; Maddox, C.; Chang, M.-C.O.; Maldonado, H.; Sarder, S.; Weber, R.J.; Robinson, A.L.; et al. Detailed Speciation of Intermediate Volatility and Semivolatile Organic Compound Emissions from Gasoline Vehicles: Effects of Cold-Starts and Implications for Secondary Organic Aerosol Formation. *Environ. Sci. Technol.* **2018**, *53*, 1706–1714. [[CrossRef](#)] [[PubMed](#)]
2. Derwent, R.G. Representing Organic Compound Oxidation in Chemical Mechanisms for Policy-Relevant Air Quality Models under Background Troposphere Conditions. *Atmosphere* **2020**, *11*, 171. [[CrossRef](#)]
3. Baltensperger, U. Aerosols in Clearer Focus. *Science* **2010**, *329*, 1474–1475. [[CrossRef](#)] [[PubMed](#)]
4. Donato, A.; Feudo, T.L.; Marinoni, A.; Dinoi, A.; Avolio, E.; Merico, E.; Calidonna, C.R.; Contini, D.; Bonasoni, P. Characterization of In Situ Aerosol Optical Properties at Three Observatories in the Central Mediterranean. *Atmosphere* **2018**, *9*, 369. [[CrossRef](#)]
5. Chen, N.; Zhao, Y.; Lyu, R.; Wu, R.; Dai, L.; Zhao, Y.; Chen, F.; Zhang, J.; Yu, H.; Guan, M. Seasonal and spatial variations of optical properties of light absorbing carbon and its influencing factors in a typical polluted city in Yangtze River Delta, China. *Atmos. Environ.* **2019**, *199*, 45–54. [[CrossRef](#)]
6. Moise, T.; Flores, J.M.; Rudich, Y. Optical Properties of Secondary Organic Aerosols and Their Changes by Chemical Processes. *Chem. Rev.* **2015**, *115*, 4400–4439. [[CrossRef](#)]
7. Nakayama, T.; Matsumi, Y.; Sato, K.; Imamura, T.; Yamazaki, A.; Uchiyama, A. Laboratory studies on optical properties of secondary organic aerosols generated during the photooxidation of toluene and the ozonolysis of  $\alpha$ -pinene. *J. Geophys. Res. Space Phys.* **2010**, *115*. [[CrossRef](#)]
8. Nakayama, T.; Sato, K.; Matsumi, Y.; Imamura, T.; Yamazaki, A.; Uchiyama, A. Wavelength and NO<sub>x</sub> dependent complex refractive index of SOAs generated from the photooxidation of toluene. *Atmos. Chem. Phys.* **2013**, *13*, 531–545. [[CrossRef](#)]
9. Li, K.; Wang, W.; Ge, M.F.; Li, J.; Wang, D. Optical properties of secondary organic aerosols generated by photooxidation of aromatic hydrocarbons. *Sci. Rep.* **2014**, *4*, 4922. [[CrossRef](#)]
10. Li, K.; Li, J.; Wang, W.; Li, J.; Peng, C.; Wang, D.; Ge, M. Effects of Gas-Particle Partitioning on Refractive Index and Chemical Composition of m-Xylene Secondary Organic Aerosol. *J. Phys. Chem. A* **2018**, *122*, 3250–3260. [[CrossRef](#)]
11. Langridge, J.M.; Richardson, M.S.; Lack, D.A.; Brock, C.A.; Murphy, D.M. Limitations of the Photoacoustic Technique for Aerosol Absorption Measurement at High Relative Humidity. *Aerosol Sci. Technol.* **2013**, *47*, 1163–1173. [[CrossRef](#)]
12. Varma, R.M.; Ball, S.M.; Brauers, T.; Dorn, H.-P.; Heitmann, U.; Jones, R.L.; Platt, U.; Pöhler, D.; Ruth, A.A.; Shillings, A.J.L.; et al. Light extinction by secondary organic aerosol: An intercomparison of three broadband cavity spectrometers. *Atmos. Meas. Tech.* **2013**, *6*, 6685–6727. [[CrossRef](#)]
13. Zhao, W.X.; Dong, M.L.; Chen, W.D.; Gu, X.J.; Hu, C.J.; Gao, X.M.; Huang, W.; Zhang, W.J. Wavelength resolved optical extinction measurements of aerosols using broad-band cavity-enhanced absorption spectroscopy over the spectral range of 445–480 nm. *Anal. Chem.* **2013**, *85*, 2260–2268. [[CrossRef](#)] [[PubMed](#)]
14. Zhao, W.; Xu, X.; Dong, M.; Chen, W.; Gu, X.; Hu, C.; Huang, Y.; Gao, X.; Huang, W.; Zhang, W. Development of a cavity-enhanced aerosol albedometer. *Atmos. Meas. Tech.* **2014**, *7*, 2551–2566. [[CrossRef](#)]
15. Xu, X.; Zhao, W.; Zhang, Q.; Wang, S.; Fang, B.; Chen, W.; Venables, D.S.; Wang, X.; Pu, W.; Wang, X.; et al. Optical properties of atmospheric fine particles near Beijing during the HOPE-J3A campaign. *Atmos. Chem. Phys.* **2016**, *16*, 6421–6439. [[CrossRef](#)]
16. Wang, S.; Zhao, W.; Xu, X.; Fang, B.; Zhang, Q.; Qian, X.; Zhang, W.; Chen, W.; Pu, W.; Wang, X. Dependence of columnar aerosol size distribution, optical properties, and chemical components on regional transport in Beijing. *Atmos. Environ.* **2017**, *169*, 128–139. [[CrossRef](#)]
17. Ge, S.; Xu, Y.; Jia, L. Effects of inorganic seeds on secondary organic aerosol formation from photochemical oxidation of acetone in a chamber. *Atmos. Environ.* **2017**, *170*, 205–215. [[CrossRef](#)]
18. Tajuelo, M.; Rodríguez, A.M.; Baeza-Romero, M.T.T.; Aranda, A.; Díaz-De-Mera, Y.; Rodríguez, D. Secondary organic aerosol formation from  $\alpha$ -methylstyrene atmospheric degradation: Role of NO level, relative humidity and inorganic seed aerosol. *Atmos. Res.* **2019**, *230*, 104631. [[CrossRef](#)]

19. Shao, P.; Tian, H.; Sun, Y.; Liu, H.; Wu, B.; Liu, S.; Liu, X.; Wu, Y.; Liang, W.; Wang, Y.; et al. Characterizing remarkable changes of severe haze events and chemical compositions in multi-size airborne particles (PM<sub>1</sub>, PM<sub>2.5</sub> and PM<sub>10</sub>) from January 2013 to 2016–2017 winter in Beijing, China. *Atmos. Environ.* **2018**, *189*, 133–144. [[CrossRef](#)]
20. Wang, J.; Zhang, J.; Liu, Z.-J.; Wu, J.; Zhang, Y.-F.; Han, S.-Q.; Zheng, X.-J.; Zhou, L.-D.; Feng, Y.-C.; Zhu, T. Characterization of chemical compositions in size-segregated atmospheric particles during severe haze episodes in three mega-cities of China. *Atmos. Res.* **2017**, *187*, 138–146. [[CrossRef](#)]
21. Sun, Z.; Duan, F.; He, K.; Du, J.; Zhu, L. Sulfate–nitrate–ammonium as double salts in PM<sub>2.5</sub>: Direct observations and implications for haze events. *Sci. Total. Environ.* **2019**, *647*, 204–209. [[CrossRef](#)] [[PubMed](#)]
22. Huang, M.; Hao, L.; Cai, S.; Gu, X.; Zhang, W.; Hu, C.; Wang, Z.; Fang, L.; Zhang, W. Effects of inorganic seed aerosols on the particulate products of aged 1,3,5-trimethylbenzene secondary organic aerosol. *Atmos. Environ.* **2017**, *152*, 490–502. [[CrossRef](#)]
23. Huang, M.; Zhang, W.; Cai, S.; Liao, Y.; Zhao, W.; Hu, C.; Gu, X.; Fang, L.; Zhang, W. Mass spectrometric study of aged benzene secondary organic aerosol in the presence of dry ammonium sulfate. *J. Atmos. Chem.* **2016**, *73*, 329–344. [[CrossRef](#)]
24. Assaf, E.; Fittschen, C. Cross section of OH radical overtone transition near 7028 cm<sup>-1</sup> and measurement of the rate constant of the reaction of OH with HO<sub>2</sub> radicals. *J. Phys. Chem. A* **2016**, *120*, 7051–7059. [[CrossRef](#)] [[PubMed](#)]
25. Feng, Z.; Huang, M.; Cai, S.; Xu, X.; Yang, Z.; Zhao, W.; Hu, C.; Gu, X.; Zhang, W. Characterization of single scattering albedo and chemical components of aged toluene secondary organic aerosol. *Atmos. Pollut. Res.* **2019**, *10*, 1736–1744. [[CrossRef](#)]
26. Bones, D.L.; Henricksen, D.K.; Mang, S.A.; Gonsior, M.; Bateman, A.P.; Nguyen, T.B.; Cooper, W.J.; Nizkorodov, S.A. Appearance of strong absorbers and fluorophores in limonene–O<sub>3</sub> secondary organic aerosol due to NH<sub>4</sub><sup>+</sup>-mediated chemical aging over long time scales. *J. Geophys. Res. Space Phys.* **2010**, *115*. [[CrossRef](#)]
27. Bueno, P.A.; Havey, D.K.; Mulholland, G.W.; Hodges, J.T.; Gillis, K.A.; Dickerson, R.R.; Zachariah, M.R. Photoacoustic Measurements of Amplification of the Absorption Cross Section for Coated Soot Aerosols. *Aerosol Sci. Technol.* **2011**, *45*, 1217–1230. [[CrossRef](#)]
28. Washenfelder, R.A.; Flores, J.M.; Brock, C.A.; Brown, S.S.; Rudich, Y. Broadband measurements of aerosol extinction in the ultraviolet spectral region. *Atmos. Meas. Tech.* **2013**, *6*, 861–877. [[CrossRef](#)]
29. Thompson, J.E.; Barta, N.; Policarpio, D.; Duvall, R. A fixed frequency aerosol albedometer. *Opt. Express* **2008**, *16*, 2191–2205. [[CrossRef](#)]
30. Miles, R.E.H.; Rudić, S.; Orr-Ewing, A.J.; Reid, J.P. Influence of Uncertainties in the Diameter and Refractive Index of Calibration Polystyrene Beads on the Retrieval of Aerosol Optical Properties Using Cavity Ring Down Spectroscopy. *J. Phys. Chem. A* **2010**, *114*, 7077–7084. [[CrossRef](#)]
31. Huang, M.; Hao, L.; Gu, X.; Hu, C.; Zhao, W.; Wang, Z.; Fang, L.; Zhang, W. Effects of inorganic seed aerosols on the growth and chemical composition of secondary organic aerosol formed from OH-initiated oxidation of toluene. *J. Atmos. Chem.* **2013**, *70*, 151–164. [[CrossRef](#)]
32. Jathar, S.H.; Mahmud, A.; Barsanti, K.C.; Asher, W.E.; Pankow, J.F.; Kleeman, M.J. Water uptake by organic aerosol and its influence on gas/particle partitioning of secondary organic aerosol in the United States. *Atmos. Environ.* **2016**, *129*, 142–154. [[CrossRef](#)]
33. Reid, J.S.; Eck, T.F.; Christopher, S.A.; Koppmann, R.; Dubovik, O.; Eleuterio, D.P.; Holben, B.N.; Reid, E.A.; Zhang, J. A review of biomass burning emissions part III: Intensive optical properties of biomass burning particles. *Atmos. Chem. Phys.* **2005**, *5*, 827–849. [[CrossRef](#)]
34. Lambe, A.T.; Chhabra, P.S.; Onasch, T.B.; Brune, W.H.; Hunter, J.F.; Kroll, J.H.; Cummings, M.J.; Brogan, J.F.; Parmar, Y.; Worsnop, D.R.; et al. Effect of oxidant concentration, exposure time, and seed particles on secondary organic aerosol chemical composition and yield. *Atmos. Chem. Phys.* **2015**, *15*, 3063–3075. [[CrossRef](#)]
35. Atkinson, R.; Arey, J. Atmospheric Degradation of Volatile Organic Compounds. *Chem. Rev.* **2003**, *103*, 4605–4638. [[CrossRef](#)]

36. Hinks, M.L.; Montoya-Aguilera, J.; Ellison, L.; Lin, P.; Laskin, A.; Laskin, J.; Shiraiwa, M.; Dabdub, D.; Nizkorodov, S.A. Effect of relative humidity on the composition of secondary organic aerosol from the oxidation of toluene. *Atmos. Chem. Phys. Online* **2018**, *18*, 1643–1652. [[CrossRef](#)]
37. Sato, K.; Takami, A.; Kato, Y.; Seta, T.; Fujitani, Y.; Hikida, T.; Shimono, A.; Imamura, T. AMS and LC/MS analyses of SOA from the photooxidation of benzene and 1,3,5-trimethyl benzene in the presence of NO<sub>x</sub>: Effects of chemical structure on SOA aging. *Atmos. Chem. Phys.* **2012**, *12*, 4667–4682. [[CrossRef](#)]
38. Suh, I.; Zhang, R.; Molina, L.T.; Molina, M.J. Oxidation Mechanism of Aromatic Peroxy and Bicyclic Radicals from OH-Toluene Reactions. *J. Am. Chem. Soc.* **2003**, *125*, 12655–12665. [[CrossRef](#)]
39. Carlton, A.G.; Turpin, B.; Altieri, K.E.; Seitzinger, S.; Reff, A.; Lim, H.-J.; Ervens, B. Atmospheric oxalic acid and SOA production from glyoxal: Results of aqueous photooxidation experiments. *Atmos. Environ.* **2007**, *41*, 7588–7602. [[CrossRef](#)]
40. Laskin, J.; Laskin, J.; Nizkorodov, S.A. Chemistry of Atmospheric Brown Carbon. *Chem. Rev.* **2015**, *115*, 4335–4382. [[CrossRef](#)]
41. Updyke, K.M.; Nguyen, T.B.; Nizkorodov, S.A. Formation of brown carbon via reactions of ammonia with secondary organic aerosols from biogenic and anthropogenic precursors. *Atmos. Environ.* **2012**, *63*, 22–31. [[CrossRef](#)]
42. Kampf, C.J.; Jakob, R.; Hoffmann, T. Identification and characterization of aging products in the glyoxal/ammonium sulfate system-implications for light-absorbing material in atmospheric aerosols. *Atmos. Chem. Phys.* **2012**, *12*, 6323–6333. [[CrossRef](#)]
43. Lee, A.K.Y.; Zhao, R.; Li, R.; Liggio, J.; Li, S.-M.; Abbatt, J.P.D. Formation of Light Absorbing Organo-Nitrogen Species from Evaporation of Droplets Containing Glyoxal and Ammonium Sulfate. *Environ. Sci. Technol.* **2013**, *47*, 12819–12826. [[CrossRef](#)] [[PubMed](#)]
44. Maxut, A.; Mechakra, H.; Nozière, B.; Fenet, B. Formation mechanisms and yields of small imidazoles from reactions of glyoxal with NH<sub>4</sub><sup>+</sup> in water at neutral pH. *Phys. Chem. Chem. Phys.* **2015**, *17*, 20416–20424. [[CrossRef](#)]
45. Gao, Y.; Wang, H.; Zhang, X.; Jing, S.; Peng, Y.; Qiao, L.; Zhou, M.; Huang, D.D.; Wang, Q.; Li, X.; et al. Estimating Secondary Organic Aerosol Production from Toluene Photochemistry in a Megacity of China. *Environ. Sci. Technol.* **2019**, *53*, 8664–8671. [[CrossRef](#)]
46. Liu, Y.; Liggio, J.; Staebler, R.; Li, S.-M. Reactive uptake of ammonia to secondary organic aerosols: Kinetics of organonitrogen formation. *Atmos. Chem. Phys.* **2015**, *15*, 13569–13584. [[CrossRef](#)]
47. Trainic, M.; Riziq, A.A.; Lavi, A.; Flores, J.M.; Rudich, Y. The optical, physical and chemical properties of the products of glyoxal uptake on ammonium sulfate seed aerosols. *Atmos. Chem. Phys.* **2011**, *11*, 9697–9707. [[CrossRef](#)]
48. Pósfai, M.; Xu, H.; Anderson, J.R.; Buseck, P.R. Wet and dry sizes of atmospheric aerosol particles: An AFM-TEM Study. *Geophys. Res. Lett.* **1998**, *25*, 1907–1910. [[CrossRef](#)]
49. Cruz, C.N.; Pandis, S.N. Deliquescence and Hygroscopic Growth of Mixed Inorganic-Organic Atmospheric Aerosol. *Environ. Sci. Technol.* **2000**, *34*, 4313–4319. [[CrossRef](#)]
50. Meyer, N.K.; Duplissy, J.; Gysel, M.; Metzger, A.; Dommen, J.; Weingartner, E.; Alfarra, M.R.; Fletcher, C.; Good, N.; McFiggans, G.; et al. Analysis of the hygroscopic and volatile properties of ammonium sulphate seeded and un-seeded SOA particles. *Atmos. Chem. Phys.* **2008**, *8*, 8629–8659. [[CrossRef](#)]
51. Hallquist, M.; Wenger, J.; Baltensperger, U.; Rudich, Y.; Simpson, D.; Claeys, M.; Dommen, J.; Donahue, N.M.; George, C.; Goldstein, A.H.; et al. The formation, properties and impact of secondary organic aerosol: Current and emerging issues. *Atmos. Chem. Phys.* **2009**, *9*, 5155–5236. [[CrossRef](#)]
52. Lu, Z.; Hao, J.; Takekawa, H.; Hu, L.; Li, J. Effect of high concentrations of inorganic seed aerosols on secondary organic aerosol formation in the m-xylene/NO<sub>x</sub> photooxidation system. *Atmos. Environ.* **2009**, *43*, 897–904. [[CrossRef](#)]

